

1                   Low-Pressure and Nascent Yields of Stabilized Criegee

2                   Intermediates  $\text{CH}_2\text{OO}$  and  $\text{CH}_3\text{CHOO}$  in Ozonolysis of Propene

3                   *Lei Yang, Mixtli Campos-Pineda,<sup>§</sup> Katia Hatem, and Jingsong Zhang<sup>\*</sup>*

4                   Department of Chemistry

5                   University of California, Riverside

6                   Riverside, CA 92521

7                   USA

8

9                   <sup>§</sup> Present address: Centre for Research into Atmospheric Chemistry, University College Cork,  
10                   T12 YN60, Ireland.

11                   \* Corresponding author. Email: [jingsong.zhang@ucr.edu](mailto:jingsong.zhang@ucr.edu); Tel +1 951 827 4197; Fax: +1 951 827  
12                   4713. Also at Air Pollution Research Center, University of California, Riverside, California  
13                   92521, United States.

14

15                   **Keywords:** ozonolysis, propene, Criegee intermediate, cavity ringdown spectroscopy

16

1    **Abstract**

2    The yields of stabilized Criegee intermediates (sCIs), both  $\text{CH}_2\text{OO}$  and  $\text{CH}_3\text{CHOO}$ , produced from  
3    ozonolysis of propene at low pressures (7-16 Torr) were measured indirectly using cavity  
4    ringdown spectroscopy (CRDS) and chemical titration with an excess amount of sulfur dioxide  
5    ( $\text{SO}_2$ ). The method of monitoring the consumption of  $\text{SO}_2$  as a scavenger and the production of  
6    secondary formaldehyde (HCHO) allows characterization of the total sCI and the stabilized  
7     $\text{CH}_2\text{OO}$  yields at low pressure and in short residence time. Both the total sCI and the stabilized  
8     $\text{CH}_2\text{OO}$  yields in the propene ozonolysis were found to decrease with decreasing pressure. By  
9    extrapolating the 7-16 Torr measurements to zero-pressure limit, the nascent yield of the total sCIs  
10   was determined to be  $25 \pm 2\%$ . The ranges of nascent yields of stabilized  $\text{CH}_2\text{OO}$  and stabilized  
11    $\text{CH}_3\text{CHOO}$  were estimated to be 20-25% and 0-5%, respectively. The branching ratios of the  
12   stabilized and high-energy  $\text{CH}_2\text{OO}^*$  and  $\text{CH}_3\text{CHOO}^*$  were also determined.

13

1      **Introduction**

2      As one of the major oxidation pathways of unsaturated volatile organic carbons (VOCs) in  
3      Earth's troposphere, ozonolysis plays an critical role in the formation of hydroxyl radical (OH)  
4      and the production of secondary organic aerosol (SOA).<sup>1-4</sup> The first step in the mechanism of  
5      ozonolysis involves the addition of ozone (O<sub>3</sub>) to the olefinic bond of alkene, which produces a  
6      chemically activated five-membered ring called primary ozonide (POZ). POZ then undergoes a  
7      prompt decomposition, through cleavage of an O–O and a C–C bond, into a carbonyl compound

8      and a carbonyl oxide known as Criegee intermediate (CI).<sup>5</sup> A small fraction of POZ may isomerize  
9      into ketohydroperoxide (KHP) and decompose into dialdehyde, OH radicals and other products.<sup>6</sup>

10     <sup>9</sup> With multiple resonance structures (zwitterion structures and biradical electronic configurations),  
11     CI has a rich reactivity and is the least stable among all its isomers.<sup>10, 11</sup> As ozonolysis reaction is

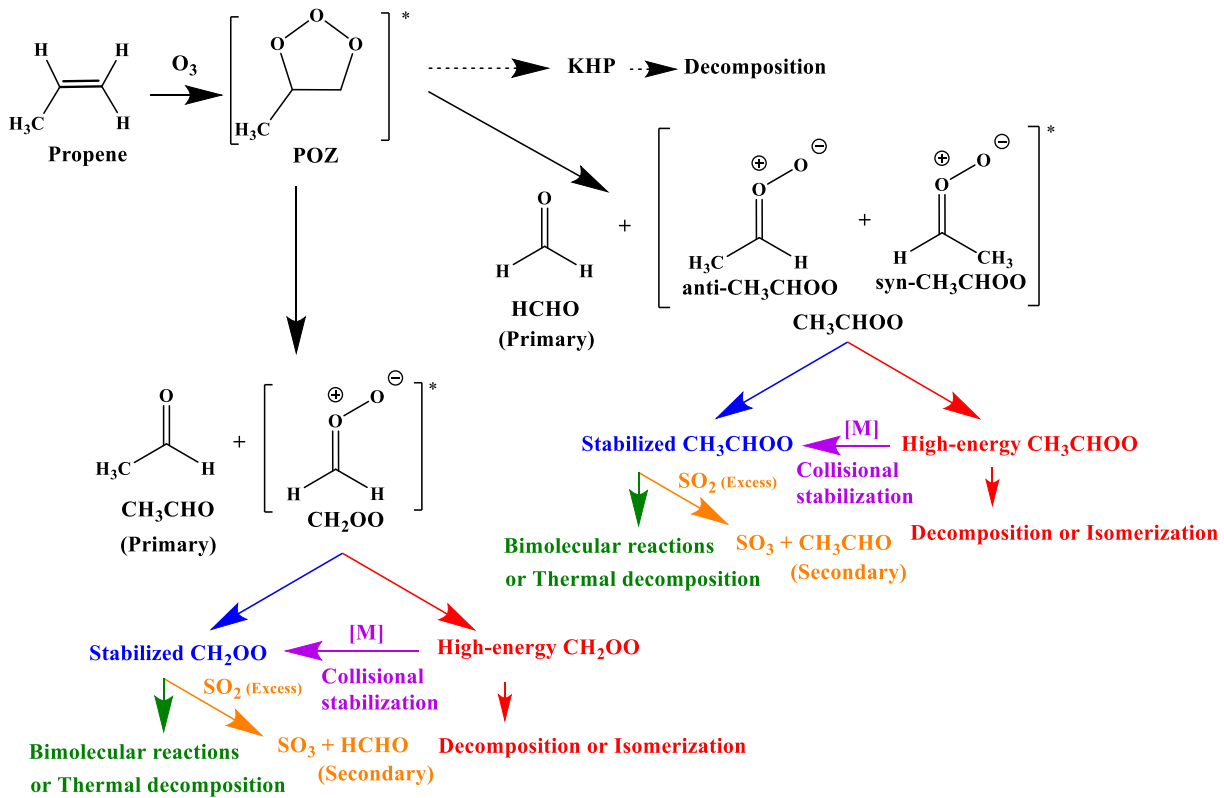
12     highly exothermic, CIs are produced with broad internal energy distributions.<sup>12</sup> High-energy CIs  
13     born with enough internal energy to surmount the isomerization or dissociation barriers can  
14     transform rapidly into dioxirane or vinyl hydroperoxide, and then decompose into OH radical,

15     organic radicals, and other products on nanosecond timescales.<sup>13</sup> While stabilized Criegee  
16     intermediates (sCIs) are born with less energy, and have a longer lifetime to get involved in  
17     bimolecular reactions with atmospheric species or to undergo thermal decomposition.<sup>14</sup> The  
18     branching ratio of the high-energy CIs and sCIs depends both on the internal energy distributions  
19     and the heights of the dissociation or isomerization energy barriers of the CIs.

20     CIs have transient lifetimes in the troposphere because the rate coefficients for ozonolysis are  
21     small, while the unimolecular and bimolecular consumption reactions of CIs are rapid.<sup>11</sup> Owing to  
22     the low steady-state concentrations of CIs produced from ozonolysis, decades' efforts have proven  
23     the difficulty in detecting CIs directly in gas phase. In 2012, Welz and co-workers developed a

1 new method to synthesize high-concentration sCIs in gas phase by using photolysis of  
2 diiodo-alkane in an excess amount of oxygen.<sup>15</sup> Since then, direct laboratory measurements on the  
3 unimolecular and bimolecular kinetics of sCIs have been reported.<sup>16-22</sup> However, the yields of the  
4 high-energy CIs and sCIs in ozonolysis of alkenes, which are related to the energy distributions of  
5 CIs and the branching ratio of various pathways in the reaction network of CIs, can only be  
6 measured in actual ozonolysis reactions. To measure the yield of sCIs in ozonolysis, chemical  
7 titration methods have been developed by using a scavenger to selectively and effectively react  
8 with all the sCIs produced from ozonolysis. Among the various molecules that have been studied  
9 and utilized as the sCI scavenger previously (such as hexafluoroacetone (HFA), formic acid  
10 (HCOOH), methanol (CH<sub>3</sub>OH), formaldehyde (HCHO), water (H<sub>2</sub>O) and carbon monoxide  
11 (CO)),<sup>23, 24</sup> sulfur dioxide (SO<sub>2</sub>) is a commonly used scavenger in recent studies because of the  
12 characterizable spectral features of SO<sub>2</sub> or the end products (sulfuric acid (H<sub>2</sub>SO<sub>4</sub>))<sup>25-28</sup> or  
13 carbonyls<sup>29</sup> as well as the rapid reaction between SO<sub>2</sub> and sCIs (for example, IUPAC  
14 recommended  $k$  (SO<sub>2</sub> + CH<sub>2</sub>OO) =  $3.7 \times 10^{-11}$  cm<sup>3</sup> molecule<sup>-1</sup> s<sup>-1</sup>),<sup>30</sup> which allows SO<sub>2</sub> to capture  
15 all the sCIs before the thermal decomposition or other biomolecular reaction of sCIs. The total  
16 amount of sCIs is then determined by measuring either the amount of end products or the  
17 consumption of the scavenger ( $\Delta[\text{SO}_2]$ ).<sup>31-34</sup>

18 The production of sCIs can be from the direct dissociation of POZ, or from the collisional  
19 stabilization of the high-energy CIs. For example, as shown in the reaction network of propene  
20 ozonolysis in Scheme 1, the stabilized CH<sub>2</sub>OO and CH<sub>3</sub>CHOO (blue) come from the  
21 decomposition reaction of POZ as well as the thermalization of high-energy CH<sub>2</sub>OO\* and  
22 CH<sub>3</sub>CHOO\* after their deactivation collisions with other molecules (purple). As such, the yield of  
23 sCIs in ozonolysis of acyclic alkenes are dependent on pressure. Measuring the nascent yield of



**Scheme 1.** Simplified reaction network of propene ozonolysis with an excess amount of  $\text{SO}_2$  scavenger.

1 sCIs at zero-pressure limit is important for understanding the original energy profile of the  
 2 ozonolysis of alkenes and the nascent energy distribution of CIs, which has attracted significant  
 3 theoretical interest.<sup>6,35</sup> However, even though the nascent yield of sCIs is an important benchmark  
 4 for the reaction dynamics calculations and kinetics studies of CIs, most research on sCIs to date  
 5 have focused on the atmospheric-pressure region,<sup>28, 29, 36</sup> considering the difficulty and relatively  
 6 larger uncertainty in determining sCI yields at low pressure. The sCI yields at the atmospheric  
 7 pressure are attributed to a combination of factors, including the direct decomposition of POZ and  
 8 the collisional stabilization of high-energy CIs. As a result, how the specific branching ratio of the  
 9 different CIs evolve in this process remains a challenging topic.

10 In this work, we present a systematic study on the nascent and low-pressure yields of stabilized

1 CH<sub>2</sub>OO and CH<sub>3</sub>CHOO produced from the ozonolysis of propene. Cavity ringdown spectroscopy  
2 (CRDS) in the near-UV region was used to quantify sCIs by monitoring the consumption of the  
3 added titrant SO<sub>2</sub> and the production of secondary HCHO. Spectral features of SO<sub>2</sub>, O<sub>3</sub>, and HCHO  
4 were fitted with their reference cross sections to obtain the number densities. The yields of sCIs in  
5 the ozonolysis of propene were measured at different low pressures from 7-16 Torr, and then the  
6 nascent yields of stabilized CH<sub>2</sub>OO and CH<sub>3</sub>CHOO were determined by extrapolation to the zero  
7 pressure. The branching ratio of the stabilized and high-energy CH<sub>2</sub>OO\* and CH<sub>3</sub>CHOO\* were  
8 also determined from the experiment.

9

10 **Experimental methods**

11 The average concentration of the targeted species was determined based on the following  
12 equation (1).

$$13 \quad \alpha = \sum_i \sigma_i(\lambda) N_i + f(\lambda) = \frac{L}{cl_s} \left( \frac{1}{\tau} - \frac{1}{\tau_0} \right) \quad (1)$$

14 which involves the following parameters: the absorption coefficient ( $\alpha$ ), the absorption cross-  
15 section of each species at different wavelengths ( $\sigma_i(\lambda)$ ), the number density of each absorber ( $N_i$ ),  
16 the distance between the two mirrors ( $L = 100$  cm), the speed of light ( $c$ ), the sample length ( $l_s =$   
17 57 cm), the ringdown time when absorber species are in the cavity ( $\tau$ ), the ringdown time in empty  
18 cavity ( $\tau_0$ ), and parameter  $f(\lambda)$  which accounts for the unidentified broad extinction contribution  
19 at different wavelengths. As shown in Figure S1 in Electronic Supplementary Information (ESI),  
20 ozonolysis reactions were carried out in a cylindrical quartz flow cell with a sample length of 57  
21 cm and diameter of 2.54 cm, which was used as a fast flow reactor. A mixture of propene and N<sub>2</sub>  
22 dilution gas was introduced into the reactor and combined with O<sub>3</sub> (~1% in O<sub>2</sub>) generated by an

1 ozone generator. In cases where the confirmation of sCI identity or sCI yield measurements were  
2 required,  $\text{SO}_2$  (~4% in  $\text{N}_2$ ) was mixed with propene prior to the introduction of  $\text{O}_3$  to scavenge  
3 sCIs. To generate 10 Hz laser pulses in the range of 647-651 nm, a Lambda-Physik dye laser using  
4 DCM dye in methanol was pumped by a Continuum Surelite II Nd:YAG laser at 532 nm. The  
5 second harmonic was produced by an Inrad Autotracker III in the range of 323.5-325.5 nm. A pair  
6 of highly reflective mirrors centered at 330 nm (>99.9%, Layertec GmbH) was used to establish a  
7 baseline ringdown time ( $\tau_0$ ) of approximately 5  $\mu\text{s}$ . With the long effective optical path and high  
8 sensitivity ( $\alpha_{min} \sim 3 \times 10^{-8} \text{ cm}^{-1}$ ), CRDS was capable of measuring signals from low-concentration  
9 species. The flow parameters of the reactor are listed in Table S1 in ESI, which shows that the  
10 radial diffusion in the flow cell can be ignored under our experimental conditions and the flow  
11 reactor can be reasonably modelled as a plug flow reactor (PFR) using the Kintecus software  
12 package<sup>37</sup>.

13 As shown in Figure 1 and Figure S2, the UV spectra (black lines) of the ozonolysis reaction  
14 (propene +  $\text{O}_3$ ) at 323.5-325.2 nm were analyzed by fitting the spectral features of  $\text{O}_3$  and  $\text{HCHO}$   
15 (red lines) to determine the final concentration of  $\text{O}_3$  ( $[\text{O}_3]_f$ ) and the initial concentration of primary  
16  $\text{HCHO}$  ( $[\text{HCHO}]_i$ ). While in the titration reaction (propene +  $\text{O}_3$  +  $\text{SO}_2$ ), the spectral signatures of  
17  $\text{O}_3$ ,  $\text{HCHO}$ , and  $\text{SO}_2$  can also be isolated from some broad background contributions of secondary  
18 reactions (Figure 1 and Figure S3), enabling the determination of the final concentrations of  $\text{SO}_2$   
19 and  $\text{HCHO}$  ( $[\text{SO}_2]_f$  and  $[\text{HCHO}]_f$  (from both primary and secondary  $\text{HCHO}$ ), and the  $\text{O}_3$   
20 concentration ( $[\text{O}_3]_f$ ) remained unchanged with or without  $\text{SO}_2$ ). The initial  $\text{O}_3$  and  $\text{SO}_2$   
21 concentrations ( $[\text{O}_3]_i$  and  $[\text{SO}_2]_i$ ) were measured by using nitrogen ( $\text{N}_2$ ) to replace the  
22 corresponding reactants (alkene or  $\text{O}_3$ ) under the same flow conditions. To ensure the accuracy of  
23 the measurement, reference cross sections of  $\text{O}_3$ ,  $\text{SO}_2$ , and  $\text{HCHO}$  were carefully selected from the

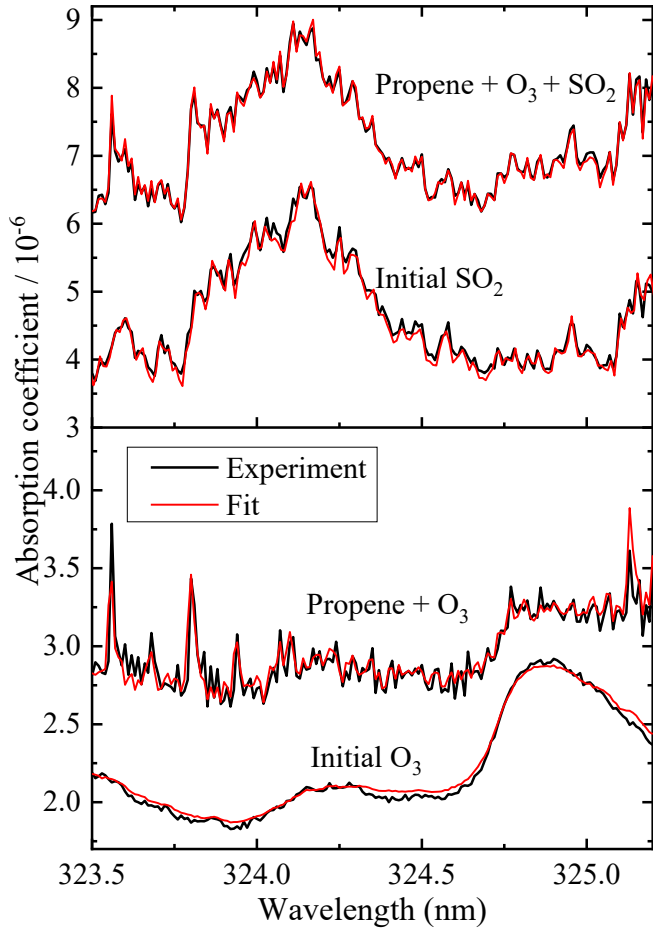


**Figure 1.** Representative near-UV CRDS spectra (black) in ozonolysis of propene (propene + O<sub>3</sub>) and the titration reaction with SO<sub>2</sub> (propene + O<sub>3</sub> + SO<sub>2</sub>), along with the fitted spectra using the corresponding reference cross sections (red). Concentrations of the reactants and products in this example (unit: molecules cm<sup>-3</sup>): [O<sub>3</sub>]<sub>i</sub> = 1.59 × 10<sup>14</sup>, [propene]<sub>i</sub> = 9.97 × 10<sup>16</sup>, [O<sub>3</sub>]<sub>f</sub> = 9.00 × 10<sup>13</sup>, [SO<sub>2</sub>]<sub>i</sub> = 3.66 × 10<sup>14</sup>, [SO<sub>2</sub>]<sub>f</sub> = 3.45 × 10<sup>14</sup>, [HCHO]<sub>i</sub> (the sharp features in propene + O<sub>3</sub>) = 4.2 × 10<sup>13</sup>, [HCHO]<sub>f</sub> (in propene + O<sub>3</sub> + SO<sub>2</sub>) = 5.7 × 10<sup>13</sup>. The total pressure was 10 Torr. The residence time inside the flow reactor was 0.92 s. All experiments were carried out at room temperature.

1 MPI Mainz UV/vis Spectral Atlas<sup>38</sup> based on the appropriate wavelength ranges and spectral  
 2 resolution. These reference cross sections were then fitted to our experimental spectra, allowing  
 3 for the creation of custom references that effectively minimized any differences in measurement  
 4 sensitivities. This approach was particularly important for HCHO, as its rovibronic features could

1 be influenced by various energy distributions during ozonolysis reaction and potentially shifted in  
2 the experimental spectra.

3 As the reaction rate coefficient  $k$  ( $\text{OH} + \text{propene}$ ) ranges from  $2.5\text{--}2.9 \times 10^{-11} \text{ cm}^3 \text{ molecule}^{-1} \text{ s}^{-1}$   
4 at 7–760 Torr and 298K, the large excess amount of propene present in the reaction mixture  
5 (approximately  $1.0 \times 10^{17} \text{ molecules cm}^{-3}$ ) can rapidly react with the OH radicals produced by  
6 ozonolysis and completely deplete them. In the meantime, sCIs were scavenged by  $\text{SO}_2$  with fast  
7 reaction rate coefficients, for example,  $k(\text{CH}_2\text{OO} + \text{SO}_2) = 3.7 \times 10^{-11} \text{ cm}^3 \text{ molecule}^{-1} \text{ s}^{-1}$ ,  $k(\text{syn-CH}_3\text{CHOO} + \text{SO}_2) = 2.6 \times 10^{-11} \text{ cm}^3 \text{ molecule}^{-1} \text{ s}^{-1}$  and  $k(\text{anti-CH}_3\text{CHOO} + \text{SO}_2) = 1.4 \times 10^{-10} \text{ cm}^3 \text{ molecule}^{-1} \text{ s}^{-1}$ . When the amount of  $\text{SO}_2$  present in the reaction mixture was in a large excess  
8 compared to the total amount of sCIs (for example, in this work  $[\text{SO}_2]_i \sim 3.5 \times 10^{14} \text{ molecules cm}^{-3}$ ), all sCIs produced in ozonolysis can be captured by  $\text{SO}_2$ , and the amount of consumed  $\text{SO}_2$  was  
9 equal to the amount of sCIs. Therefore, the total yield of sCIs can be determined by the following  
10 equation (2).

$$14 \quad 15 \quad \text{Yield of sCI} = \frac{\Delta[\text{SO}_2]}{\Delta[\text{O}_3]} \quad (2)$$

16 where the amount of consumed  $\text{SO}_2$  is  $\Delta[\text{SO}_2] = [\text{SO}_2]_i - [\text{SO}_2]_f$  and the amount of consumed  $\text{O}_3$  is  
17  $\Delta[\text{O}_3] = [\text{O}_3]_i - [\text{O}_3]_f$ .

18 At the same time,  $\text{HCHO}$  and  $\text{SO}_3$  were produced in the reaction between  $\text{CH}_2\text{OO}$  and  $\text{SO}_2$  as  
19 the major pathway, while the reaction between  $\text{CH}_3\text{CHOO}$  and  $\text{SO}_2$  produced  $\text{CH}_3\text{CHO}$  and  $\text{SO}_3$   
20 after the decomposition of the chemically-activated secondary ozonide (SOZ) at low pressure.<sup>21</sup>,  
21 <sup>39–41</sup> The amount of secondary  $\text{HCHO}$  produced after adding  $\text{SO}_2$ ,  $\Delta[\text{HCHO}] = [\text{HCHO}]_f - [\text{HCHO}]_i$ ,  
22 is thus related to the amount of stabilized  $\text{CH}_2\text{OO}$ . Therefore, the yield of stabilized  $\text{CH}_2\text{OO}$  can  
23 be determined by the following equation (3), and the yield of stabilized  $\text{CH}_3\text{CHOO}$  is equal to the  
24

1 difference of the total yield of sCIs and the yield of stabilized CH<sub>2</sub>OO. Since bimolecular reactions  
2 of CH<sub>2</sub>OO might also produce HCHO before SO<sub>2</sub> was added, the  $\Delta[\text{HCHO}]/\Delta[\text{O}_3]$  measured with  
3 this method should be considered as a lower limit of the stabilized CH<sub>2</sub>OO yield.

4

5 Yield of stabilized CH<sub>2</sub>OO  $\geq \frac{\Delta[\text{HCHO}]}{\Delta[\text{O}_3]}$  (3)

6

7 As shown in Scheme 1, the production of the total amount of CH<sub>2</sub>OO and CH<sub>3</sub>CHOO  
8 intermediates from initial decomposition of POZ in propene ozonolysis are equal to that of the  
9 corresponding primary carbonyl products, CH<sub>3</sub>CHO and HCHO, respectively. Thus, the total yield  
10 of CH<sub>3</sub>CHOO (including *syn/anti*-conformers in the full internal energy profile) is equal to the  
11 yield of the primary HCHO, and can be determined by calculating the ratio of the amount of HCHO  
12 produced in ozonolysis ( $[\text{HCHO}]_i$ ) and the consumed O<sub>3</sub> ( $\Delta[\text{O}_3]$ ), as shown in equation (4). Note  
13 that in propene ozonolysis at the atmospheric pressure, the total yields of carbonyls were measured  
14 to be in the range of 100% to 110%,<sup>36,42</sup> with CH<sub>2</sub>OO, CH<sub>3</sub>CHOO, or KHP possibly producing a  
15 small amount of secondary HCHO; thus in this system, the measured  $[\text{HCHO}]_i$  should be  
16 considered as the upper limit for the primary HCHO. Our kinetic model estimates the extent of  
17 this overestimation, as discussed in ESI (see Table S2-S5).

18 Yield of CH<sub>3</sub>CHOO  $\leq \frac{[\text{HCHO}]_i}{\Delta[\text{O}_3]}$  (4)

19 Theoretical calculations showed that 12% of POZ produced in ethene ozonolysis can isomerize  
20 into KHP,<sup>6</sup> yet there is no reported study on propene ozonolysis to date. Assuming the KHP  
21 branching in propene ozonolysis also up to 12%, the total yield of CH<sub>2</sub>OO (including both  
22 stabilized CH<sub>2</sub>OO and high-energy CH<sub>2</sub>OO<sup>\*</sup>) can be obtained by subtracting the yield of primary  
23 HCHO (the total yield of CH<sub>3</sub>CHOO) from the total CI yield of 88-100%. Thus, using the

1 equations listed above and the relationships indicated in Scheme 1, the yields of stabilized  $\text{CH}_2\text{OO}$ ,  
2 high-energy  $\text{CH}_2\text{OO}^*$ , stabilized  $\text{CH}_3\text{CHOO}$ , and high-energy  $\text{CH}_3\text{CHOO}^*$  can all be obtained  
3 using the near-UV CRDS and the  $\text{SO}_2$  titration method.

4 Equation 2 is valid when the concentration of  $\text{SO}_2$  is high enough to completely react  
5 with/scavenge all the sCIs produced from the ozonolysis reaction, before the sCIs can undergo any  
6 further unimolecular or bimolecular reactions with other species such as the  $\text{O}_3$ , alkene, or  $\text{HCHO}$   
7 in the system. However, it should be noted that using too much  $\text{SO}_2$  may also cause saturation of  
8 the absorption spectra and limit the accuracy of the measurements. This is because CRDS has a  
9 limited dynamic range in measurement, typically 2 orders of magnitude. Therefore, exceeding the  
10 upper limit of the dynamic range would result in a rapid increase of the ringdown decay rate,  
11 leading to signal saturation and noisy measurements. To avoid using an excessively high  
12 concentration of  $\text{SO}_2$ , which could also lead to the formation of secondary products and an increase  
13 in the broad background in the absorption spectra, a titration curve was measured as shown in  
14 Figure 2, which allowed for the determination of the minimum amount of  $\text{SO}_2$  required to  
15 completely consume all the sCIs. The titration curve was obtained by measuring the change in the  
16 ratio of consumed  $\text{SO}_2$  to consumed  $\text{O}_3$  ( $\Delta[\text{SO}_2]/\Delta[\text{O}_3]$ ) as the initial concentration of  $\text{SO}_2$  was  
17 varied under identical conditions of pressure, residence time, and initial propene and  $\text{O}_3$   
18 concentrations. This approach ensured that the optimal amount of  $\text{SO}_2$  was used to titrate the sCIs  
19 while avoiding any unnecessary excess. Since  $\text{O}_3$  was the limiting reagent in the ozonolysis  
20 reaction studied in this experiment (with the propene concentration being approximately three  
21 orders of magnitude higher than the  $\text{O}_3$  concentration), the ratio of the initial concentrations of  $\text{SO}_2$   
22 and  $\text{O}_3$  was plotted on the horizontal axis. As the initial  $\text{SO}_2$  concentration increased, the ratio of  
23  $\Delta[\text{SO}_2]/\Delta[\text{O}_3]$  increased and eventually levelled off. At this plateau,  $\Delta[\text{SO}_2]/\Delta[\text{O}_3]$  approached a

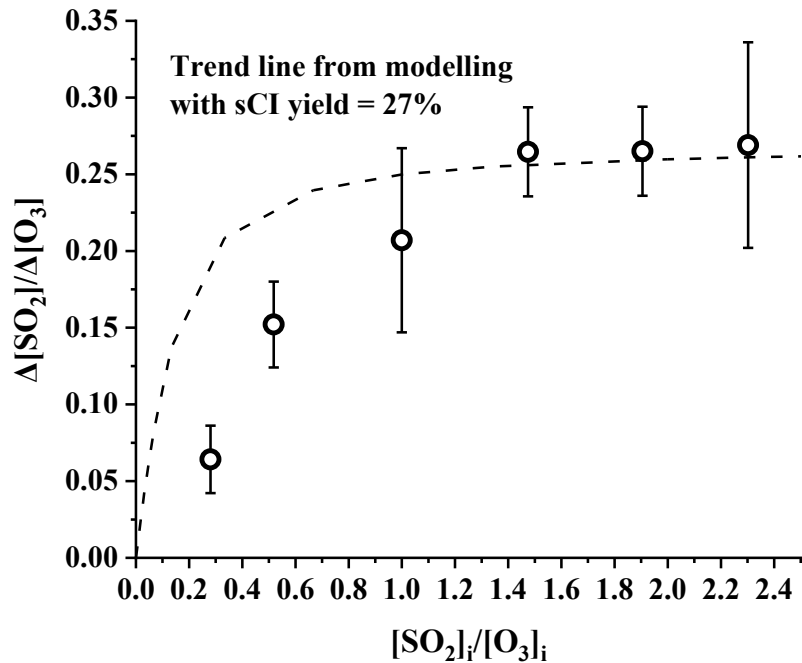


**Figure 2.** The titration curve showing the variation in the consumption of SO<sub>2</sub> in propene ozonolysis as the initial SO<sub>2</sub> concentration was varied at a total pressure of 10 Torr. The horizontal axis represents the ratio of the initial SO<sub>2</sub> concentration to the initial O<sub>3</sub> concentration, which reflects the excess extent of the SO<sub>2</sub> titrant. The initial O<sub>3</sub> concentration was kept constant at approximately  $1.5 \times 10^{14}$  molecules cm<sup>-3</sup> throughout the titration curve. The vertical axis is the ratio of the consumed amounts of SO<sub>2</sub> and O<sub>3</sub>. The curve reached a maximum of approximately 27% when concentration of the added SO<sub>2</sub> was high enough to fully titrate all the sCIs produced during propene ozonolysis. The trend line was calculated using kinetic modelling. Error bars represent one standard deviation in repeated measurements at each SO<sub>2</sub> concentration.

1 constant value, indicating the maximum consumption of SO<sub>2</sub> and completion of the titration of  
 2 sCIs. This plateau was observed at an initial [SO<sub>2</sub>]/[O<sub>3</sub>] ratio higher than 1.5, corresponding to SO<sub>2</sub>  
 3 concentration higher than  $2.3 \times 10^{14}$  molecules cm<sup>-3</sup>. Based on the consumed O<sub>3</sub> being about 40-  
 4 50% of its initial concentration and the typical yield of sCIs in ozonolysis being less than 40%, the  
 5 amount of SO<sub>2</sub> needed to reach the plateau in the titration curve was more than 10 times higher  
 6 than the total amount of sCIs produced in ozonolysis. In the sCI measurement experiments under

1 different pressures, high initial concentrations of  $\text{SO}_2$  were used with the  $[\text{SO}_2]/[\text{O}_3]$  ratio being  
2 approximately 2.3. This allowed for the efficient scavenging of sCIs via the  $\text{SO}_2 + \text{sCI}$  reactions,  
3 which have a large rate constant (e.g.,  $k(\text{SO}_2 + \text{CH}_2\text{OO}) = 3.7 \times 10^{-11} \text{ cm}^3 \text{ molecule}^{-1} \text{ s}^{-1}$ ) and  
4 ensured that the  $\text{SO}_2 + \text{sCI}$  scavenging reaction was the dominant pathway for the sCI removal,  
5 outcompeting all other reaction pathways of sCI. The titration curve was further supported by the  
6 results of kinetic modelling built for the titration reaction using the Kintecus software package,<sup>37</sup>  
7 as presented in Table S2 in ESI. The trend line of  $\Delta[\text{SO}_2]/\Delta[\text{O}_3]$  calculated from the kinetic  
8 modelling (dashed line in Figure 2) was found to be in good agreement with our experimental  
9 measurements, except for the initial part of the titration curve where the  $\text{SO}_2$  concentration was  
10 not high enough to dominate over other reaction pathways involving  $\text{CH}_2\text{OO}$  and  $\text{CH}_3\text{CHOO}$ . In  
11 the initial rising part of the curve where all reaction pathways of  $\text{CH}_2\text{OO}$  compete and are involved,  
12 the reaction kinetics is complex and harder to model accurately; whereas it becomes easier to  
13 model the plateau where  $\text{SO}_2$  is sufficient to dominate other pathways and the kinetics becomes  
14 “simple”. While the initial gap indicates that there is room to improve our kinetic model, the  
15 agreement between the kinetic model and experimental results in the plateau region helps validate  
16 the endpoint of titration (the main focus of this work). The experimental measurements on  
17  $\Delta[\text{SO}_2]/\Delta[\text{O}_3]$  in this study were subject to noticeable error bars, representing one standard  
18 deviation of repeated measurements. The extent of the reactions in the short residence time  
19 (approximately 0.9 s) was limited by the relatively slow reaction between propene and  $\text{O}_3$  ( $k$   
20 (propene +  $\text{O}_3$ ) =  $1.05 \times 10^{-17} \text{ cm}^3 \text{ molecule}^{-1} \text{ s}^{-1}$ ). Despite the relatively large error bars, it was  
21 crucial to maintain a short residence time of less than 1 second to prevent accumulation of  
22 secondary products such as formic acids, carbonyls, and SOA. These byproducts can not only  
23 contribute to a broad UV absorption background and decrease detection sensitivity but also

1 compete with  $\text{SO}_2$  in the reaction with sCIs, as observed in our experiments and confirmed by  
2 kinetic modelling calculations.

3

4

5 **Results and discussion**

6 As propene is an asymmetric alkene, its ozonolysis produces formaldehyde oxide ( $\text{CH}_2\text{OO}$ ) and  
7 *syn/anti* conformers of acetaldehyde oxide (*syn/anti*- $\text{CH}_3\text{CHOO}$ ). Figure 3 shows the total yield  
8 of sCIs and the yield of stabilized  $\text{CH}_2\text{OO}$  produced from ozonolysis of propene in the pressure  
9 range of 7-16 Torr. The initial  $[\text{SO}_2]_i/[\text{O}_3]_i$  ratio was kept at 2.3-2.5 to ensure that sCIs can be  
10 scavenged completely at all the pressures. The linear fit of the trend shows that the total sCI yield  
11 decreases slightly from 28% to 26% when the pressure decreases from 16 to 7 Torr. The nascent  
12 yield of total sCIs in propene ozonolysis is determined to be  $25 \pm 2\%$  after extrapolation to the  
13 zero-pressure limit. The yield of secondary HCHO after adding  $\text{SO}_2$  (the lower limit of the  
14 stabilized  $\text{CH}_2\text{OO}$ ) also showed a small decrease with decreasing pressure in the 7-16 Torr region,  
15 and the lower limit of the nascent yield of stabilized  $\text{CH}_2\text{OO}$  is  $20 \pm 2\%$  at zero pressure. The  
16 uncertainty of the nascent yields was estimated from the standard error of the weighted linear fit  
17 using the least-squares method and corrected with the critical value in 95% confidence *t*-test (more  
18 details in the description of Table S6 and Table S7 in ESI). The yield of HCHO in ozonolysis of  
19 propene was measured to be  $62 \pm 5\%$ , which contains both primary HCHO yield and small  
20 secondary HCHO yield produced from other pathways. According to our kinetic modelling, the  
21 yield of secondary HCHO produced from the  $\text{CH}_2\text{OO}$  bimolecular reactions is  $\leq 5\%$  and there  
22 could be  $\sim 3\%$  additional HCHO from the KHP decomposition (see Table S3). Thus, the total yield  
23 of *syn/anti* conformers of  $\text{CH}_3\text{CHOO}$  determined from the primary yield of HCHO from equation

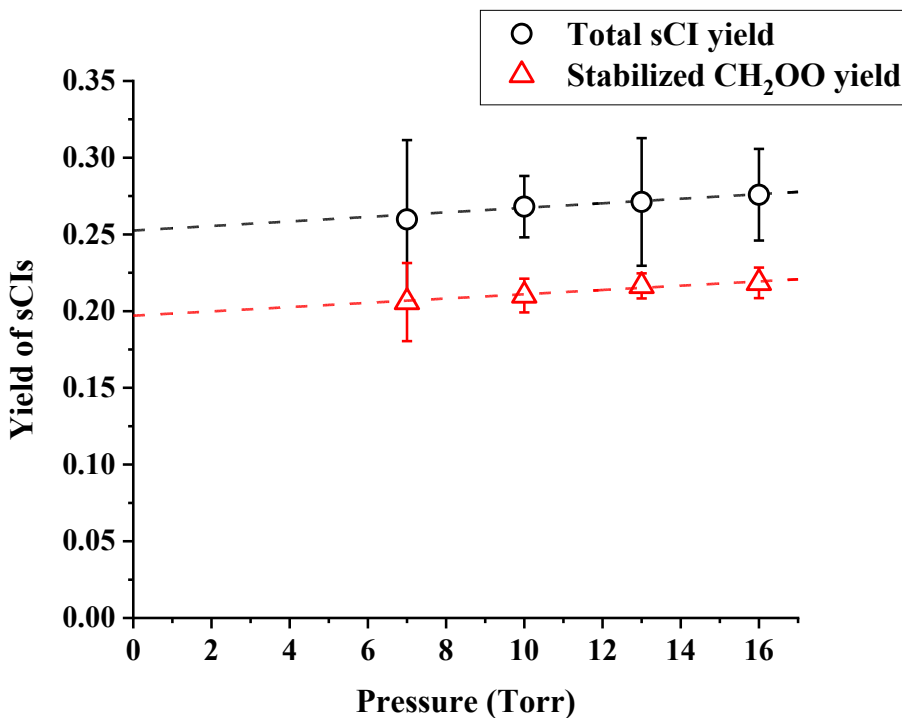


**Figure 3.** Low-pressure yield of sCIs (stabilized CH<sub>2</sub>OO and CH<sub>3</sub>CHOO) produced in ozonolysis of propene measured below 16 Torr. Total sCI yield (black) was determined from the consumption of SO<sub>2</sub>, while the yield of stabilized CH<sub>2</sub>OO (red) was calculated from the production of secondary HCHO after adding SO<sub>2</sub>. The dashed lines represent the weighted linear fit of the experimental data points and are extrapolated to the zero-pressure limit. Error bars represent one standard deviation in repeated measurements at each pressure.

1 (4) is estimated to be in a range of 54-62%, and the total yield of CH<sub>2</sub>OO is 29-43% (assuming 0-  
 2 12% of KHP yield from the POZ decomposition).<sup>6</sup> From these results, the nascent yields of  
 3 stabilized CH<sub>2</sub>OO and stabilized CH<sub>3</sub>CHOO are calculated to be 20-25% and 0-5%, while the  
 4 nascent yield of the high-energy CH<sub>2</sub>OO\* and high-energy CH<sub>3</sub>CHOO\* are 9-18% and 53-57%,  
 5 respectively. The specific values of the CI yields under different assumptions are listed in Table  
 6 S3.

7 The yield of HCHO in ozonolysis reported here,  $62 \pm 5\%$ , is consistent with the previous studies  
 8 of 60-65% yield at the atmospheric pressure,<sup>29, 36, 42-44</sup> which indicates that pressure may not have

1 a large impact on the branching ratio of the total CH<sub>2</sub>OO and CH<sub>3</sub>CHOO produced from  
2 decomposition of POZ in propene ozonolysis. However, the energy distribution of CIs and the  
3 total sCI yield are dependent on the pressure. In the previous studies at the atmospheric pressure,  
4 the total yield of sCIs in propene ozonolysis has been determined to be 44%, 25 ± 2% and 34 ±  
5 1% by Horie et al.,<sup>36</sup> Hatakeyama et al.<sup>28</sup> and Newland et al,<sup>29</sup> respectively. Among these studies,  
6 Hatakeyama et al.<sup>28</sup> and Newland et al.<sup>29</sup> used SO<sub>2</sub> as the scavenger and quantified either the  
7 associated product H<sub>2</sub>SO<sub>4</sub> or the consumed SO<sub>2</sub>, respectively, while Horie et al.<sup>36</sup> added HCHO as  
8 the scavenger and measured the adduct between sCIs and HCHO. Our experimental value of the  
9 total nascent sCI yield at the zero pressure, 25 ± 2%, is about 9% lower than the 34 ± 1 %  
10 atmospheric sCI yield in propene ozonolysis reported by Newland et al.<sup>29</sup>, who used the same  
11 scavenger and quantification method ( $\Delta[\text{SO}_2]$  for total sCIs) with this work. Newland et al.<sup>29</sup> also  
12 reported the yield of stabilized CH<sub>2</sub>OO in propene ozonolysis being 23% at the atmospheric  
13 pressure, measured from the increase of secondary HCHO after adding SO<sub>2</sub> as in the current work.  
14 The nascent yield of stabilized CH<sub>2</sub>OO measured in this work is about 3% lower than the  
15 atmospheric yield, yet both of them should be considered as lower limits because secondary HCHO  
16 were already produced from bimolecular reactions of CH<sub>2</sub>OO prior to adding SO<sub>2</sub>.

17 From the ratio between the nascent yield of stabilized CH<sub>2</sub>OO (20-25%) and the total yield of  
18 CH<sub>2</sub>OO (29-43%), the nascent stabilization factor of CH<sub>2</sub>OO is determined to be 52-74%. The  
19 specific values of the CI stabilization factors under different assumptions are listed in Table S3.  
20 Newland et al.<sup>29</sup> reported the stabilization factor of CH<sub>2</sub>OO to be 60% at atmospheric pressure,  
21 calculated from the ratio between the lower limit of stabilized CH<sub>2</sub>OO yield (23%) and the initial  
22 CH<sub>3</sub>CHO yield of 38%. Thus, if taking the same method, the nascent stabilization factor of CH<sub>2</sub>OO  
23 at low pressure in this work is ~8% lower than that at atmospheric pressure. Similarly, the nascent

1 stabilization factor of  $\text{CH}_3\text{CHOO}$  can be estimated to be 0-9% at the zero pressure limit, and it is  
2 about 9-30% lower than that at the atmospheric pressure.<sup>29</sup> This observation agrees with the  
3 relatively low nascent yield of stabilized  $\text{CH}_3\text{CHOO}$  of 0-5% measured in ozonolysis of *trans*-2-  
4 butene and *cis*-2-butene.<sup>32, 33</sup> Compared to  $\text{CH}_3\text{CHOO}$ ,  $\text{CH}_2\text{OO}$  has a much higher stabilization  
5 factor because of its high isomerization barriers to form dioxirane and hydroperoxide (reported to  
6 be 18.2–19.1 and 30.8–31.8 kcal/mol, respectively),<sup>12, 35</sup> while the *syn*-conformers of the larger  
7 sCIs can undergo a lower barrier pathway through the 1,4-hydrogen migration to form alkenyl  
8 hydroperoxide, and this process is enhanced by tunnelling (barrier of *syn*- $\text{CH}_3\text{CHOO}$  to form vinyl  
9 hydroperoxide is 17.05 kcal/mol).<sup>11, 12, 45</sup>

10 Compared to the 20% nascent yield of sCIs in ethene ozonolysis,<sup>34</sup> the total nascent sCI yield in  
11 propene ozonolysis is about 5% higher. Although the nascent stabilized  $\text{CH}_2\text{OO}$  yield is about the  
12 same in propene and ethene ozonolysis (~ 20%), considering that the branching ratio of the  $\text{CH}_2\text{OO}$   
13 pathway from POZ is only ~29-43% in propene ozonolysis (while it is 88-100% in ethene  
14 ozonolysis), the nascent stabilization factor of  $\text{CH}_2\text{OO}$  is 29-54% higher in propene ozonolysis  
15 compared to that in ethene ozonolysis. Assuming the internal energy is distributed evenly on POZ,  
16 after the cleavage of POZ, energy taken away by the carbonyl coproduct would increase with the  
17 increase of its size. The acetaldehyde ( $\text{CH}_3\text{CHO}$ ) coproduct of  $\text{CH}_2\text{OO}$  in propene ozonolysis can  
18 take away more internal energy than the  $\text{HCHO}$  coproduct of  $\text{CH}_2\text{OO}$  in ethene ozonolysis, and  
19 thus the mean internal energy of  $\text{CH}_2\text{OO}$  in propene ozonolysis is lower than that in ethene  
20 ozonolysis.

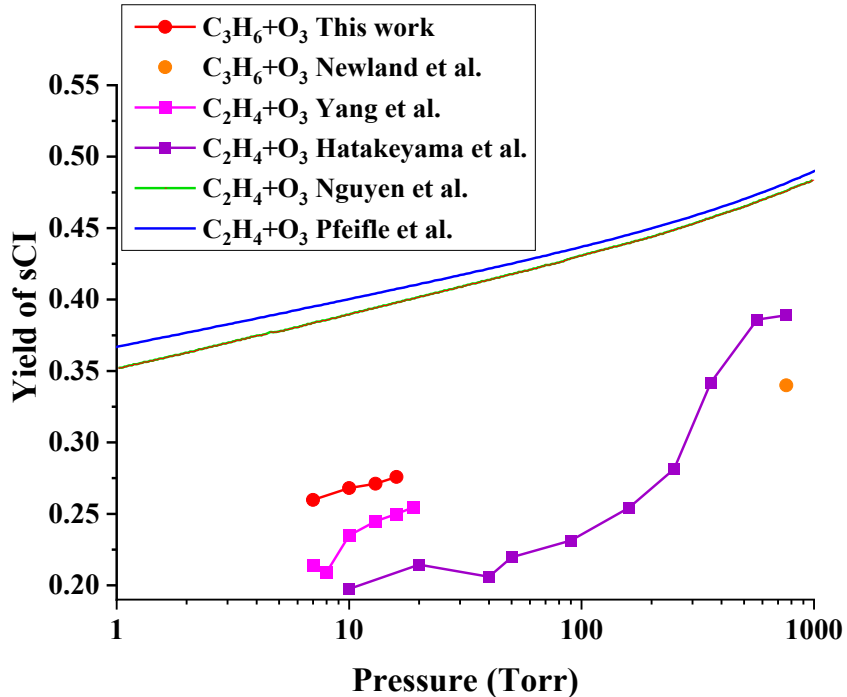


**Figure 4.** The total sCI yield in propene ozonolysis measured by experimental works compared to the sCI yields reported by experimental and theoretical works for the ethene ozonolysis.<sup>6, 25, 29, 34, 35</sup>

Previous theoretical calculations suggest that the collisional stabilization of POZ in ozonolysis of alkene is negligible,<sup>35</sup> and that the pressure-dependent behavior of sCI yields is due to collisional stabilization of high-energy CIs with buffer gases. In Figure 4, the low-pressure sCI yields measured by this work is compared to the sCI yields measured by Newland et al.<sup>29</sup> at atmospheric pressure and the increasing trend of sCI yields reported by experimental and theoretical works for ethene ozonolysis at 1-1000 Torr.<sup>6, 25, 34, 35</sup> Although the alkenes are different, the general trends are similar to those by theoretical predictions with respect to the logarithmic pressure.<sup>6, 35</sup> The sCI yields calculated by Nguyen et al.<sup>35</sup> were based on statistical energy partitioning, while those by Pfeifle et al.<sup>6</sup> were from trajectory models (non-statistical theories). A few other theoretical works on ozonolysis support the nonergodic and nonstatistical behaviors of energy partitioning in the

1 ozonolysis reactions of propene and vinyl ethers.<sup>46, 47</sup> Compared to the previous experimental  
2 studies on ethene ozonolysis,<sup>25, 34</sup> the increase of sCI yield is smaller in propene ozonolysis at 7-  
3 760 Torr, which might suggest a smaller collisional stabilization effect of CH<sub>3</sub>CHOO than CH<sub>2</sub>OO.  
4 By comparing the predictions from the theoretical models with the experimental results, future  
5 researchers can assess the accuracy and reliability of their models and potentially refine them to  
6 better describe the behavior of CIs.

7

8

## 9 **Conclusions**

10 The yields of the total sCIs, the stabilized CH<sub>2</sub>OO, and the stabilized CH<sub>3</sub>CHOO produced in  
11 ozonolysis of propene were determined at low pressures from 7 to 16 Torr by monitoring the  
12 consumption of SO<sub>2</sub> scavenger as well as the production of secondary HCHO using the near-UV  
13 CRDS. Nascent yields of these sCIs were obtained from extrapolation to the zero-pressure limit,  
14 and the branching ratio of the stabilized and high-energy CH<sub>2</sub>OO\* and CH<sub>3</sub>CHOO\* were also  
15 determined. CH<sub>2</sub>OO has a higher nascent stabilization factor than CH<sub>3</sub>CHOO due to its relatively  
16 higher energy barrier for isomerization and dissociation. The nascent stabilization factor of  
17 CH<sub>2</sub>OO is higher in propene ozonolysis than in ethene ozonolysis, because the larger size of the  
18 carbonyl co-product in propene ozonolysis can take away more energy. The branching ratio  
19 obtained from the current study can be used as benchmarks for future theoretical calculations.

20

21

## 22 **Electronic Supplementary Information (ESI)**

23 The Supplementary Information is available free of charge. The Supplementary Information  
24 provides more experimental and modelling details. Figures S1–S4 present the experimental setup,

1 the broad absorption background  $f(\lambda)$  in the spectra, and the comparison between modelling and  
2 experimental sCI yields in propene ozonolysis. Tables S1–S8 list flow parameters of the reactor,  
3 kinetic modelling, summarized nascent CI/carbonyl yields based on different assumptions, and sCI  
4 yields measurements at each pressure.

5

6

7 **Conflicts of Interest**

8 There are no conflicts of interest to declare.

9

10

11 **Acknowledgements**

12 This work was supported by the U.S. National Science Foundation (CHE-2155232). L. Yang  
13 acknowledges the support from a UC Riverside Dissertation Research Grant. M. Campos-Pineda  
14 acknowledges the support from a UCMEXUS-CONTACYT Doctoral Fellowship.

15

16

17 **Notes and references**

- 18 1. S. E. Paulson and J. J. Orlando, *Geophys. Res. Lett.*, 1996, **23**, 3727-3730.
- 19 2. B. J. Finlayson-Pitts and J. N. Pitts, *Chemistry of the Upper and Lower Atmosphere: Theory,*  
20 *Experiments, and Applications*, Academic Press, San Diego, 2000.
- 21 3. R. Atkinson and J. Arey, *Chem. Rev.*, 2003, **103**, 4605-4638.
- 22 4. J. H. Kroll and J. H. Seinfeld, *Atmos. Environ.*, 2008, **42**, 3593-3624.
- 23 5. R. Criegee, *Angew. Chem., Int. Ed. Engl.*, 1975, **14**, 745-752.

1 6. M. Pfeifle, Y. T. Ma, A. W. Jasper, L. B. Harding, W. L. Hase and S. J. Klippenstein, *J.*  
2 *Chem. Phys.*, 2018, **148**, 174306.

3 7. A. C. Rousso, N. Hansen, A. W. Jasper and Y. Ju, *J. Phys. Chem. A*, 2018, **122**, 8674-8685.

4 8. N. Genossar, J. P. Porterfield and J. H. Baraban, *Phys. Chem. Chem. Phys.*, 2020, **22**,  
5 16949-16955.

6 9. C. S. Lewin, O. Herbinet, G. A. Garcia, P. Arnoux, L.-S. Tran, G. Vanhove, L. Nahon, F.  
7 Battin-Leclerc and J. Bourgalais, *Chem. Commun.*, 2022, **58**, 13139-13142.

8 10. C. A. Taatjes, *Annu. Rev. Phys. Chem.*, 2017, **68**, 183-207.

9 11. D. L. Osborn and C. A. Taatjes, *Int. Rev. Phys. Chem.*, 2015, **34**, 309-360.

10 12. M. Olzmann, E. Kraka, D. Cremer, R. Gutbrod and S. Andersson, *J. Phys. Chem. A*, 1997,  
11 **101**, 9421-9429.

12 13. G. T. Drozd, T. Kurtén, N. M. Donahue and M. I. Lester, *J. Phys. Chem. A*, 2017, **121**,  
13 6036-6045.

14 14. J. Jr-Min Lin and W. Chao, *Chem. Soc. Rev.*, 2017, **46**, 7483-7497.

15 15. O. Welz, J. D. Savee, D. L. Osborn, S. S. Vasu, C. J. Percival, D. E. Shallcross and C. A.  
16 Taatjes, *Science*, 2012, **335**, 204-207.

17 16. J. D. Fenske, A. S. Hasson, A. W. Ho and S. E. Paulson, *J. Phys. Chem. A*, 2000, **104**,  
18 9921-9932.

19 17. O. Welz, A. J. Eskola, L. Sheps, B. Rotavera, J. D. Savee, A. M. Scheer, D. L. Osborn, D.  
20 Lowe, A. Murray Booth, P. Xiao, M. Anwar H. Khan, C. J. Percival, D. E. Shallcross and  
21 C. A. Taatjes, *Angew. Chem., Int. Ed.*, 2014, **53**, 4547-4550.

22 18. F. Liu, J. M. Beames, A. S. Petit, A. B. McCoy and M. I. Lester, *Science*, 2014, **345**, 1596-  
23 1598.

1 19. Y. Liu, K. D. Bayes and S. P. Sander, *J. Phys. Chem. A*, 2014, **118**, 741-747.

2 20. Y.-P. Lee, *J. Chem. Phys.*, 2015, **143**, 020901.

3 21. C. A. Taatjes, O. Welz, A. J. Eskola, J. D. Savee, A. M. Scheer, D. E. Shallcross, B.

4 Rotavera, E. P. F. Lee, J. M. Dyke, D. K. W. Mok, D. L. Osborn and C. J. Percival, *Science*,

5 2013, **340**, 177-180.

6 22. L. Sheps, *J. Phys. Chem. Lett.*, 2013, **4**, 4201-4205.

7 23. G. T. Drozd and N. M. Donahue, *J. Phys. Chem. A*, 2011, **115**, 4381-4387.

8 24. G. T. Drozd, J. Kroll and N. M. Donahue, *J. Phys. Chem. A*, 2011, **115**, 161-166.

9 25. S. Hatakeyama, H. Kobayashi, Z. Y. Lin, H. Takagi and H. Akimoto, *J. Phys. Chem.*, 1986,

10 **90**, 4131-4135.

11 26. J. P. Hakala and N. M. Donahue, *J. Phys. Chem. A*, 2016, **120**, 2173-2178.

12 27. T. Berndt, R. Kaethner, J. Voigtländer, F. Stratmann, M. Pfeifle, P. Reichle, M. Sipilä, M.

13 Kulmala and M. Olzmann, *Phys. Chem. Chem. Phys.*, 2015, **17**, 19862-19873.

14 28. S. Hatakeyama, H. Kobayashi and H. Akimoto, *J. Phys. Chem.*, 1984, **88**, 4736-4739.

15 29. M. J. Newland, B. S. Nelson, A. Munoz, M. Rodenas, T. Vera, J. Tarrega and A. R. Rickard,

16 *Phys. Chem. Chem. Phys.*, 2020, **22**, 13698-13706.

17 30. R. A. Cox, M. Ammann, J. N. Crowley, H. Herrmann, M. E. Jenkin, V. F. McNeill, A.

18 Mellouki, J. Troe and T. J. Wallington, *Atmos. Chem. Phys.*, 2020, **20**, 13497-13519.

19 31. M. J. Newland, A. R. Rickard, L. Vereecken, A. Muñoz, M. Ródenas and W. J. Bloss,

20 *Atmos. Chem. Phys.*, 2015, **15**, 9521-9536.

21 32. M. Campos-Pineda and J. Zhang, *Sci. China Chem.*, 2018, **61**, 850–856.

22 33. M. Campos-Pineda and J. Zhang, *Chem. Phys. Lett.*, 2017, **683**, 647-652.

23 34. L. Yang, M. Campos-Pineda and J. Zhang, *J. Phys. Chem. Lett.*, 2022, **13**, 11496-11502.

1 35. T. L. Nguyen, H. Lee, D. A. Matthews, M. C. McCarthy and J. F. Stanton, *J. Phys. Chem. A*, 2015, **119**, 5524-5533.

2

3 36. O. Horie and G. K. Moortgat, *Atmos. Environ.*, 1991, **25**, 1881-1896.

4 37. J. C. Ianni, in *Computational Fluid and Solid Mechanics 2003*, ed. K. J. Bathe, Elsevier

5 Science Ltd., Oxford, 2003, pp. 1368-1372.

6 38. H. Keller-Rudek, G. K. Moortgat, R. Sander and R. Sorensen, *Earth Syst. Sci. Data*, 2013,

7 **5**, 365-373.

8 39. Y. Y. Wang, M. R. Dash, C. Y. Chung and Y. P. Lee, *J. Chem. Phys.*, 2018, **148**, 064301.

9 40. L. Vereecken, H. Harder and A. Novelli, *Phys. Chem. Chem. Phys.*, 2012, **14**, 14682-14695.

10 41. K. T. Kuwata, E. J. Guinn, M. R. Hermes, J. A. Fernandez, J. M. Mathison and K. Huang,

11 *J. Phys. Chem. A*, 2015, **119**, 10316-10335.

12 42. E. C. Tuazon, S. M. Aschmann, J. Arey and R. Atkinson, *Environ. Sci. Technol.*, 1997, **31**,

13 3004-3009.

14 43. E. Grosjean, J. B. de Andrade and D. Grosjean, *Environ. Sci. Technol.*, 1996, **30**, 975-983.

15 44. A. R. Rickard, D. Johnson, C. D. McGill and G. Marston, *J. Phys. Chem. A*, 1999, **103**,

16 7656-7664.

17 45. T. A. Stephenson and M. I. Lester, *Int. Rev. Phys. Chem.*, 2020, **39**, 1-33.

18 46. G. Vayner, S. V. Addepalli, K. Song and W. L. Hase, *J. Chem. Phys.*, 2006, **125**, 014317.

19 47. L. M. M. Quijano and D. A. Singleton, *J. Am. Chem. Soc.*, 2011, **133**, 13824-13827.

20